Synthesis, Crystal Structure, Spectroscopic Properties, and Hirshfeld Surface Analysis of Diaqua [3,14-dimethyl-2,6,13,17 tetraazatricyclo(16.4.0.0^{7,12})docosane]copper(II) Dibromide

Sunghwan Jeon [1], Ján Moncol [2], Milan Mazúr [3], Marián Valko [3,*] and Jong-Ha Choi [1,*]

[1]   Department of Chemistry, Andong National University, Andong 36729, Korea
[2]   Department of Inorganic Chemistry, Faculty of Chemical and Food Technology, Slovak University of Technology, 81237 Bratislava, Slovakia
[3]   Department of Physical Chemistry, Faculty of Chemical and Food Technology, Slovak University of Technology, 81237 Bratislava, Slovakia
*   Correspondence: marian.valko@stuba.sk (M.V.); jhchoi@anu.ac.kr (J.-H.C.)
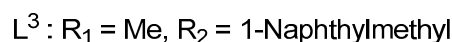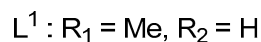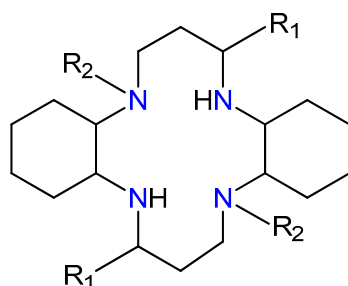
Abstract: A newly prepared Cu(II) complex salt, Cu(L^1)(H$_2$O)$_2$Br$_2$, where L^1 is 3,14-dimethyl-2,6,13,17-tetraazatricyclo(16.4.0.0^{7,12}) docosane, is characterized by elemental and crystallographic analyses. The Cu(II) center is coordinated by four nitrogen atoms of macrocyclic ligand and the axial position by two water molecules. The macrocyclic ligand adopts an optimally stable trans-III conformation with normal Cu–N bond lengths of 2.018 (3) and 2.049 (3) Å and long axial Cu1–O1W length of 2.632 (3) Å due to the Jahn–Teller effect. The complex is stabilized by hydrogen bonds formed between the O atoms of water molecules and bromide anions. The bromide anion is connected to the neighboring complex cations and water molecules through N–H···Br and O–H···Br hydrogen bonds, respectively. The g-factors obtained from the electron spin resonance spectrum show the typical trend of $g_∥ > g_⊥ >$ 2.0023, which is in a good accordance to the $d_x{}^2$-$_y{}^2$ ground state. It reveals a coordination sphere of tetragonal symmetry for the Cu(II) ion. The infrared and electronic absorption spectral properties of the complex are also discussed. Hirshfeld surface analysis represents that the H···H, H···Br/Br···H and H···O/O···H contacts are the major molecular interactions in the prepared complex.

Keywords: structural characterization; spectroscopic properties; copper(II); macrocycle; *trans*-III conformation; electron spin resonance spectroscopy; Hirshfeld surface analysis

1. Introduction

Recently, the mobilization of stem cell in bone marrow and anti-HIV effect by the cyclam derivatives and their transition metal complexes have been found [1–4]. The metal complex with the cyclam skeleton can take either trans or cis geometrical isomers because of its structural flexibility. A total of five conformational trans isomers caused by the chiral secondary amine nitrogen atoms. Furthermore, three cis-conformers are possible [5,6]. The macrocycle conformation in the complex is important factor for CXCR4 chemokine receptor recognition [1–3]. The knowledge on the coordination behavior and conformation of the cyclam derivative plays important role for development of novel and highly effective anti-HIV drugs. In this context, investigations on various constrained cyclam ligands (Scheme 1) containing cyclohexane subunits and methyl or ethyl groups have proved instructive.

L^1 : R$_1$ = Me, R$_2$ = H

L^2 : R$_1$ = Me, R$_2$ = Benzyl

L^3 : R$_1$ = Me, R$_2$ = 1-Naphthylmethyl

L^a : R$_1$ = Et, R$_2$ = H

L^b : R$_1$ = Et, R$_2$ = Benzyl
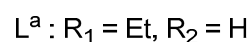
Scheme 1. Structures of various macrocyclic ligands.

The crystallographic study of $[Cu(L^1)(H_2O)_2]Cl_2$, $[Cu(L^1)(H_2O)_2](BF_4)_2 \cdot 2H_2O$, $[Cu(L^1)(ClO_4)_2]$, $[Cu(L^1)(NO_3)_2]$, $[Cu(L^1)(NO_3)_2] \cdot 3H_2O$, $[Cu(L^1)(NCS)_2] \cdot 2H_2O$, $[Cu(L^1)(NCS)]SCN$, and $[Cu(L^1)(N_3)]ClO_4 \cdot H_2O$ have been performed previously [7–14]. In these Cu(II) complexes, the macrocycles adopt the most stable trans–III conformation. The ligand containing cyclohexane ring and methyl group has sometimes showed different coordination behaviors comparing to those of the complexes with cyclam ligand. For example, crystallographic analysis of $[Cu(L^2)](ClO_4)_2$ revealed that the copper(II) ion was tetracoordinated in a square planar configuration somewhat distorted towards tetrahedral geometry [15] whereas the $[Cu(L^3)](ClO_4)_2 \cdot 2CH_3CN$ had a square planar geometry [16]. The structural and physical properties of the Cu(II) and Ni(II) complexes with macrocycles containing cyclohexane ring and ethyl group were also reported [17–22].

The structural characteristics, like chelate ring size and substituent influence the chemical properties and geometries of Cu(II) complexes. Anionic species is also an important factor in coordination chemistry, molecular assembly and medicine [23,24].

To further investigate on the effect of counter anion and water molecule to the crystal packing behavior, we report here the preparation, structural characterization, spectral properties and Hirshfeld surface analysis of a new bromide salt, $[Cu(L^1)(H_2O)_2]Br_2$, (I) (Scheme 2).
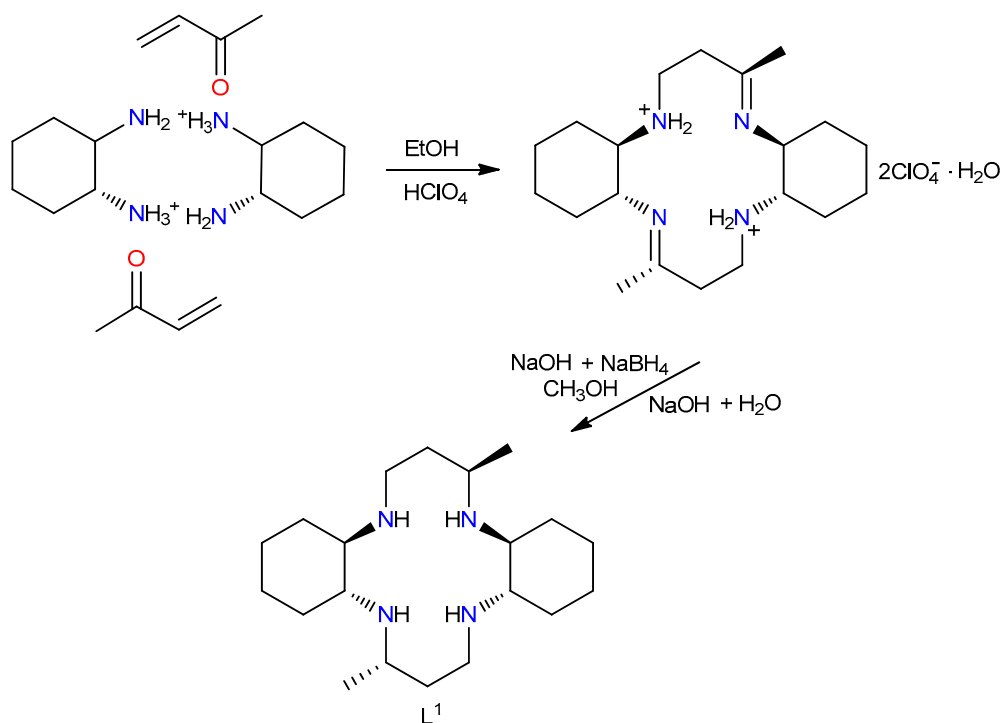

(I)
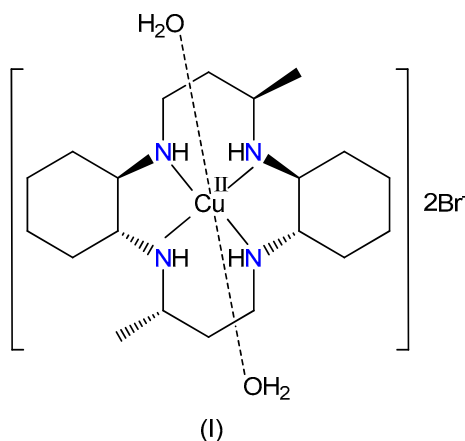
Scheme 2. Chemical structure of $[Cu(L^1)(H_2O)_2]Br_2$, (I).

2. Experimental Section

2.1. Synthesis of L^1

The macrocycle L^1 was synthesized according to a previously published procedure [25]. The synthetic process of ligand L^1 is summarized in Scheme 3.

Scheme 3. Synthetic procedure of the ligand L^1.

The yield was 88.7%. Anal. Calcd (%). for $C_{20}H_{40}N_4$: C, 71.37; H, 11.98; N, 16.65. Found (%): C, 71.63; H, 12.12; N, 16.50.

2.2. Synthesis of $[Cu(L^1)(H_2O)_2]Br_2$, (I)

A 50 mL aqueous solution of 0.5 mmol $CuBr_2$ was prepared and a 20 mL aliquot was removed, and the macrocycle L^1 (0.091 g, 0.25 mmol) was added. The resulting solution was refluxed for 60 min at 373 K. After cooling to 298 K, the pH was adjusted to 3.0 by the addition of 1.0 M HCl. Colorless and violet mixed crystals were formed from the solution over the next few days. The product mixture was added to 30 mL MeOH-acetone (1:2) solution under stirring, and the stirring was continued for 30 min at 298 K. The colorless $[H_4L^1]Cl_4 \cdot 4H_2O$ crystals was removed by filtration [26]. The filtrate was left at 298 K. After few days, violet crystals of $[Cu(L^1)(H_2O)_2]Br_2$ were given. The yield was 75.2%. The complex (I) is stable in air, and soluble in MeOH, EtOH, DMF or DMSO whereas it is insoluble in H_2O, *i*-PrOH, CH_3CN, THF and acetone. Anal. Calcd (%). for $C_{20}H_{44}CuN_4O_2Br_2$: C, 40.31; H, 7.44; N, 9.40. Found (%): C, 40.76; H, 7.40; N, 9.45.

2.3. Physical Measurements

The electronic spectrum (190–1100 nm) was recorded in a Nujol suspension using a Specord 250 Plus spectrometer (Carl Zeiss Spectroscopy GMBH, Jena, Germany). The FT-infrared spectrum was measured with a JASCO 460 FT-IR spectrometer (JASCO, Tokyo, Japan). Elemental analyses for C, H and N was carry out on a Vario MICRO cube Elemental analyzer (Elementar Analysensysteme GmbH, Langenselbold, Germany). The first derivative X-band EPR spectrum of powdered $[Cu(L^1)(H_2O)_2]Br_2$

sample was measured on an EMX EPR spectrometer (Bruker, Karlsruhe, Germany) at 298 K. The sample-containing quartz EPR tube (Bruker) was inserted inside the EPR cavity by the previously described procedure [27]. From the experimental EPR spectrum, the spin Hamiltonian parameters were found by WinEPR [28], and then refined by spectral line simulation using Bruker program SimFonia (Shareware, Bruker, Karlsruhe, Germany) [29].

2.4. Crystal Structure Analysis

Data collection and cell refinement of complex (I) were performed using a four-circle diffractometer StadiVari at 100 K. The diffractometer was equipped by HPAD detector Pilatus3R 300 K and microfocused X-ray source Genix3D Cu HF. The diffraction intensities were corrected for Lorentz and polarization factors. The structures were solved by a dual-space method using the SHELXT-2018 [30] and refined by the full matrix least-squares procedure in SHELXL-2018 [31]. Multi-scan absorption corrections were applied using Stoe LANA software (STOE & Cie GmbH, Darmstadt, Germany) [32]. Molecular graphics were drawn using DIAMOND-3 (Crystal Impact GbR, Bonn, Germany) [33]. The crystal data, data collection conditions and refinements are provided in Table 1. The crystallographic data for the complex (I) was deposited in CCDC 1912362.

Table 1. Crystal data, data collection conditions and refinements for complex (I).

Empirical formula	$C_{20}H_{44}CuN_4O_2Br_2$
Formula weight	595.95 g mol^{-1}
Temperature	100(1) K
Wavelength	1.54186 Å
Crystal system, space group	Triclinic, $P\bar{1}$
Unit cell dimensions	$a = 8.0777(4)$ Å, $\alpha = 98.879(4)°$
	$b = 8.8129(4)$ Å, $\beta = 110.204(3)°$
	$c = 10.0932(5)$ Å, $\gamma = 109.391(3)°$
Volume	650.97(5) Å^3
Z	**1**
Radiation type	Cu $K\alpha$
Density (calculated)	1.633 Mg m^{-3}
Absorption coefficient	5.31 mm^{-1}
Crystal size	$0.32 \times 0.22 \times 0.21$ mm^3
Theta range for data collection	4.9 to 70.5°
Reflections collected	19,409
Independent reflections	9304 [$R_{int} = 0.013$]
Absorption correction	Multi-scan
Max. and min. transmission	0.012 and 0.263
Refinement method	Full-matrix least-squares on F^2
Data/restraints/parameters	2241/0/134
Goodness-of-fit on $F2$	1.11
Final R indices ($F^2 > 2$)	$R_1 = 0.034$, wR_2
Extinction coefficient	0.0050(3)
Largest diff. peak and hole (e Å^{-3})	0.68 and −0.87

2.5. Hirshfeld Surface Analysis

CrystalExplorer program was used for the Hirshfeld surface analysis [34], and the normalized contact distance, d_{norm}, was mapped onto the Hirshfeld surface [35,36].

3. Results and Discussion

3.1. X-ray Crystallography

The complex (I) crystallized the triclinic space group $P\bar{1}$ with dimensions of $a = 9.2244$ (7), $b = 11.5540$ (8), $c = 12.8659$ (9) Å, and $\beta = 97.722$ (6)°. The space group of new bromide salt differed from the monoclinic space group $P2_1/c$ of $[Cu(L^1)(H_2O)_2]Cl_2$ or $P2_1/n$ of $[Cu(L^1)(H_2O)_2](BF_4)_2 \cdot 2H_2O$ with two mononuclear formula units per unit cell [7,8]. The asymmetric unit contains one half of

$[Cu(L^1)(H_2O)_2]^{2+}$ cation and one bromide anion. The important bond lengths and angles are listed in Table 2.

Figure 1 shows an ellipsoid plot (50% probability level) of the complex (I) together with the atomic numbering scheme.

Table 2. Selected bond distances (Å) and angles (°) of complex (I).

Cu1–N1	2.018 (3)	C2–C9^i	1.527 (5)
Cu1–N2	2.049 (3)	C3–C4	1.531 (4)
Cu1–O1W	2.632 (3)	C3–C8	1.526 (5)
N1–C1	1.489 (4)	C4–C5	1.528 (5)
N1–C3	1.488 (4)	C5–C6	1.516 (6)
N2–C8	1.497 (4)	C6–C7	1.528 (5)
N2–C9	1.498 (4)	C7–C8	1.525 (4)
C1–C2	1.522 (5)	C9–C10	1.521 (5)
N1–Cu1–N1^i	180.0	N1–C1–C2	110.8 (3)
N1i–Cu1–N2	95.40 (11)	C1–C2–C9^i	116.1 (3)
N1–Cu1–N2	84.60 (11)	N1–C3–C4	113.4 (3)
N1–Cu1–O1W^i	91.78 (10)	N1–C3–C8	106.4 (3)
N1–Cu1–O1W	88.22 (10)	C8–C3–C4	111.3 (3)
N2–Cu1–N2^i	180.0	C5–C4–C3	110.6 (3)
N2–Cu1–O1W	95.89 (10)	C6–C5–C4	110.8 (3)
N2–Cu1–O1W^i	84.11 (10)	C5–C6–C7	110.7 (3)
O1W^i—Cu1—O1W	180.0	C8–C7–C6	110.4 (3)
C1–N1–Cu1	116.0 (2)	N2–C8–C3	106.3 (3)
C3–N1–Cu1	108.07 (19)	N2–C8–C7	113.4 (3)
C3–N1–C1	113.4 (3)	C7–C8–C3	111.7 (3)
C8–N2–Cu1	107.20 (19)	N2–C9–C2^i	109.1 (3)
C8–N2–C9	114.6 (3)	N2—C9–C10	111.8 (3)
C9–N2–Cu1	121.0 (2)	C10–C9–C2^i	113.3 (3)

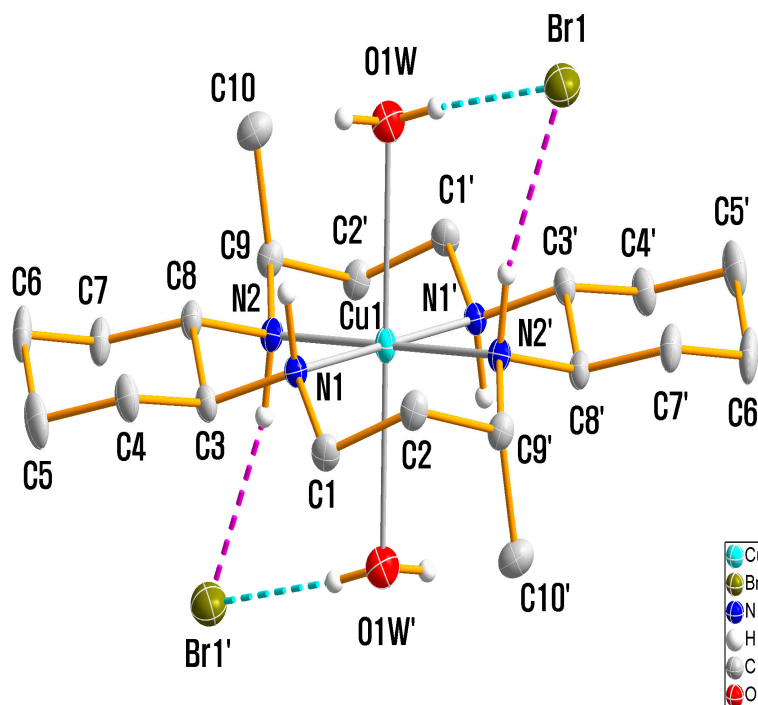Symmetry code: (i) $-x + 1$, $-y + 1$, $-z + 1$.

Figure 1. Molecular structure of complex (I).

The stereochemistry of the prepared Cu(II) complex can be considered square planar or tetragonal geometry. A semi-coordinated bond's concept was introduced to explain a situation where the axial ligands occupies the tetragonal position in a square planar Cu(II) complex with an atom in the bond

length range of 2.5–3.0 Å [36]. The Cu(II) geometry in complex (I) can be described as tetragonally distorted geometry with four N atoms from the macrocycle and two O atoms from water molecules. The macrocyclic skeleton adopted the most stable trans-III (*RRSS*) conformation. The two methyl groups on the six-membered chelate rings and the two-$(CH_2)_4$-parts of the cyclohexane backbones adopted anti configurations with respect to the macrocyclic plane. The Cu–N distances of 2.018 (3) and 2.049 (3) Å can be compared to related complexes in Table 3.

Table 3. Selected bond distances (Å) and conformations of metal complexes with macrocyclic ligands.

Compound	M–N	M–X	Conformation	Ref.
$[Cu(L^1)(H_2O)_2]Br_2$	2.018(3)–2.049(3)	2.632(3)	trans-III	This work
$[Cu(L^1)(H_2O)_2](BF_4)_2 \cdot 2H_2O$	2.028(2)–2.028(2)	2.693(3)	trans-III	[7]
$[Cu(L^1)(H_2O)_2]Cl_2$	2.017(2)–2.038(2)	2.649(2)	trans-III	[8]
$[Cu(L^1)(ClO_4)_2]$	2.005(2)–2.048(2)	2.623(2)	trans-III	[9]
$[Cu(L^1)(NO_3)_2]$	2.007(2)–2.044(2)	2.463(2)	trans-III	[10]
$[Cu(L^1)(NO_3)_2] \cdot 3H_2O$	2.021(2)–2.029(2)	2.746(2)	trans-III	[11]
$[Cu(L^1)](NCS)_2 \cdot 2H_2O$	2.020(7)–2.056(7)	3.037(7)	trans-III	[12]
$[Cu(L^1)(NCS)]SCN$	2.013(2)–2.052(2)	2.322(3)	trans-III	[13]
$[Cu(L^1)(N_3)]ClO_4 \cdot H_2O$	2.030(3)–2.054(3)	2.254(4)	trans-III	[14]
$[Cu(L^2)](ClO_4)_2$	1.990(4)–2.050(4)	3.496(3)	trans-I	[15]
$[Cu(L^2)](NO_3)_2$	1.999(7) –2.095(7)	2.964(7)	trans-III	[8]
$[Cu(L^3)](ClO_4)_2 \cdot 2CH_3CN$	2.030(3)–2.081(2)	3.264(3)	trans-III	[16]
$[Cu(L^a)(ClO_4)_2]$	2.016(2) –2.040(2)	2.762(2)	trans-III	[17]
$[Cu_x(H_{2(1-x)}L^a)(ClO_4)_2]$ ($x = 0.69$)	2.015(3) –2.047(3)	2.795(3)	trans-III	[18]
$[Cu(L^a)(NO_3)_2]$	2.014(2) –2.047(2)	2.506(2)	trans-III	[19]
$[Cu(L^a)(H_2O)_2](SCN)_2$	2.021(2) –2.046(2)	2.569(2)	trans-III	[19]
$[Ni(L^a)(NO_3)_2]$	2.051(4) –2.094(4)	2.198(3)	trans-III	[20]
$[Ni(L^a)](ClO_4)_2 \cdot 2H_2O$	1.996(7) –2.042(7)	2.973(7)	trans-III	[20]
$[Ni(L^a)(N_3)_2]$	2.070(1) –2.105(1)	2.176(1)	trans-III	[21]
$[Cu(L^b)](NO_3)_2$	2.023(2) –2.086(2)	2.936(2)	trans-III	[22]

The axial Cu1–O1W bond length [2.632(3) Å] was slightly shorter than the corresponding lengths in $[Cu(L^1)(H_2O)_2]Cl_2$ [2.649(2) Å] [7] and $[Cu(L^1)(H_2O)_2](BF_4)_2 \cdot 2H_2O$ [2.693(3) Å], but longer than that of $[Cu(L^a)(H_2O)_2](SCN)_2$ [2.569(2) Å] [19]. The Cu1–OW bond was not perpendicular to the CuN4 plane, with actual N1–Cu1–O1W and N2–Cu1–O1W angles of 88.22(11) and 95.89(11)°, respectively. The ratio of the average equatorial bond length R_S and the average axial bond length R_L was used as a measure of tetragonal distortion [36]. The ca. tetragonality factor ($T = R_S/R_L$) was 0.773, similar to the calculated mean of ca. 0.84 for those of previously reported many Cu(II) complexes [37].

The ligand L^1 contains cyclam in its backbone with two cyclohexane subunits. As it is typically observed, the five-membered chelate rings adopt a gauche conformation, whereas the six-membered rings adopt slightly distorted chair conformations due to the attached methyl group. The bond angles of the five- and six-membered chelate rings around Cu(II) were 84.60 (11) and 95.40 (11)°, respectively. The cyclohexane rings also adopted chair conformation, with the N atoms in equatorial positions. The average C–N and C–C distances, as well as the C–N–C and C–C–N angles in the macrocyclic ligands, were similar to those for a number of macrocyclic tetraamine complexes [15,16].

The supramolecular architecture involves hydrogen-bonding interactions of the N–H groups of the macrocycle ligands and O–H groups of the water molecules as donors, and the bromide anions as acceptors, resulting in a three-dimensional network structure (Figures 2 and 3). The Br$^-$ anions remain outside the coordination sphere [Cu–Br (4.768 Å)] and are connected to the semi-coordinated water molecules through O–H⋯Br (cyan) hydrogen bonds. Both hydrogens on N1 and N2 of the macrocyclic ligand were involved in very weak N–H⋯Br (pink) interactions. These hydrogen-bonded networks stabilized the crystal structure.
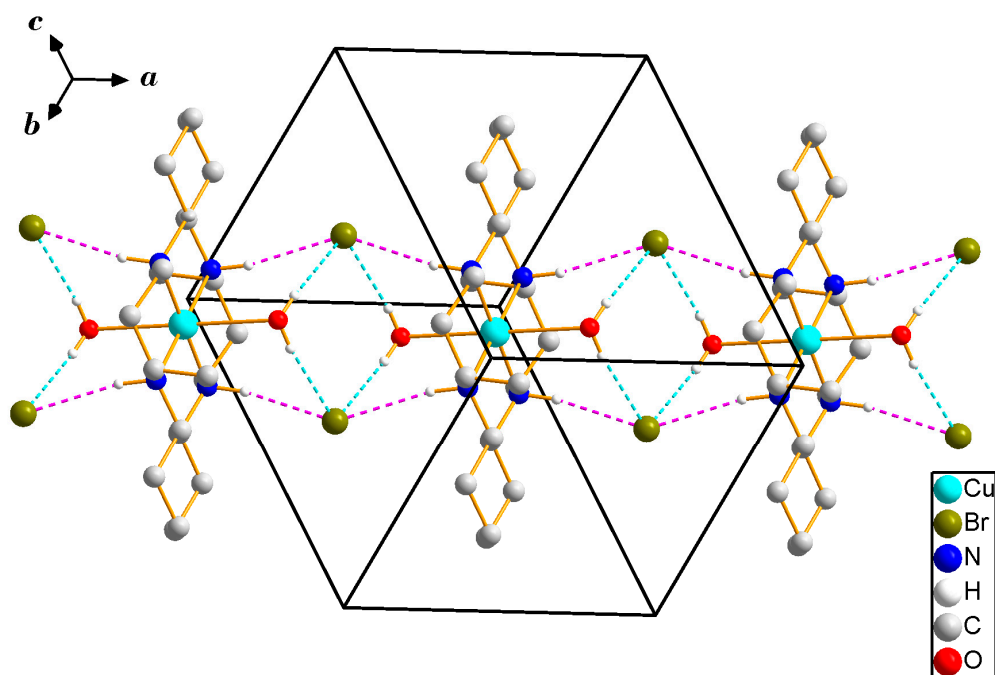
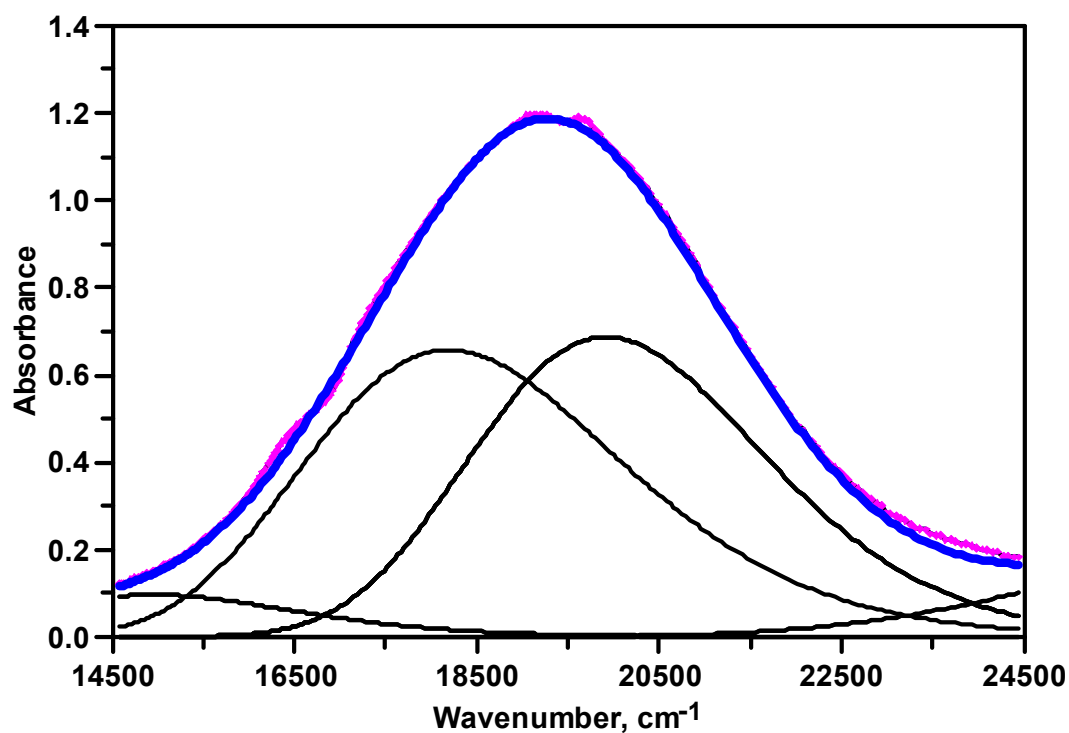**Figure 2.** Crystal packing diagram of complex (I). Dashed lines represent hydrogen bonds.

Figure 3. Visible spectrum (pink line) and resolved Gaussian curves (black line) of complex (I).

3.2. UV–Visible Spectroscopy

The electronic spectrum of complex (I) exhibited one broad *d-d* band at 19,920 cm^{-1} in the Nujol suspension. The absorption maximum, ν_{max}, is comparable to those of [Cu(L^1)(H$_2$O)$_2$](BF$_4$)$_2$·2H$_2$O, [Cu(L^1)(ClO$_4$)$_2$], and [Cu(L^a)(H$_2$O)$_2$](SCN)$_2$ with maxima at 19,570, 19,530, and 19,635 cm^{-1}, respectively [8,19]. The similar position and shape of the absorption bands reveal the presence of a CuN$_4$O$_2$ chromophore in a tetragonally elongated geometry. In complex (I), two water molecules were weakly semi-coordinated to the Cu(II) ion at the axial position. For the tetragonal geometry, the

order of one-electron energy levels is: e_g $(xz, yz) < b_{2g}$ $(xy) < a_{1g}$ $(z^2) < b_{1g}$ (x^2-y^2). The ^2D term of the free Cu(II) ion ($3d^9$) in an octahedral field splits into a higher energy $^2T_{2g}$ level and lower ^2E_g level. The ^2E_g and $^2T_{2g}$ levels for a tetragonally distorted Cu(II) complex can be further split into $^2B_{1g}$, $^2A_{1g}$, $^2B_{2g}$, and ^2E_g states. By the way, the shape of the observed *d-d* absorption band is slightly asymmetric. In order to suggest a standard model for the absorption band splitting of Cu (II) compounds of this type, the Gaussian curve (dotted line) was used to resolve into two main components as shown in Figure 3. Two maxima of the resolved bands were observed at 18,180 and 19,920 cm^{-1}, respectively. The two bands were assigned in order of increasing energy: $^2B_{1g}{\rightarrow}^2B_{2g}$ and $^2B_{1g}{\rightarrow}^2E_g$ [38]. Much weaker intensity and lower energy absorptions at 12,035 cm^{-1} arose from the $^2B_{1g}{\rightarrow}^2A_{1g}$ transition. The energy level sequence depends on the degree of tetragonal distortion due to the ligand-field effect.

3.3. Infrared Spectroscopy

The FT-IR (Fourier transform infrared) spectra of (a) the ligand L^1 and (b) its complex (I) are shown in Figure 4. Absorption band at 3494 cm^{-1} of ligand, and two peaks at 3389 and 3360 cm^{-1} of complex (I) are attributed to v(O-H) stretching vibration of the water molecules. The band at 1634 cm^{-1} can be assigned to δ(H-O-H) bending mode. The intense bands observed in the frequency region 3340–3050 and 3000–2800 cm^{-1} easily are assigned to the v(N—H) and v(C—H) stretching modes, respectively [39]. The decreased asymmetric and symmetric stretching v(N—H) frequencies compared to those of the free ligands may be due to the coordination and hydrogen bonding interaction of the secondary amine groups.
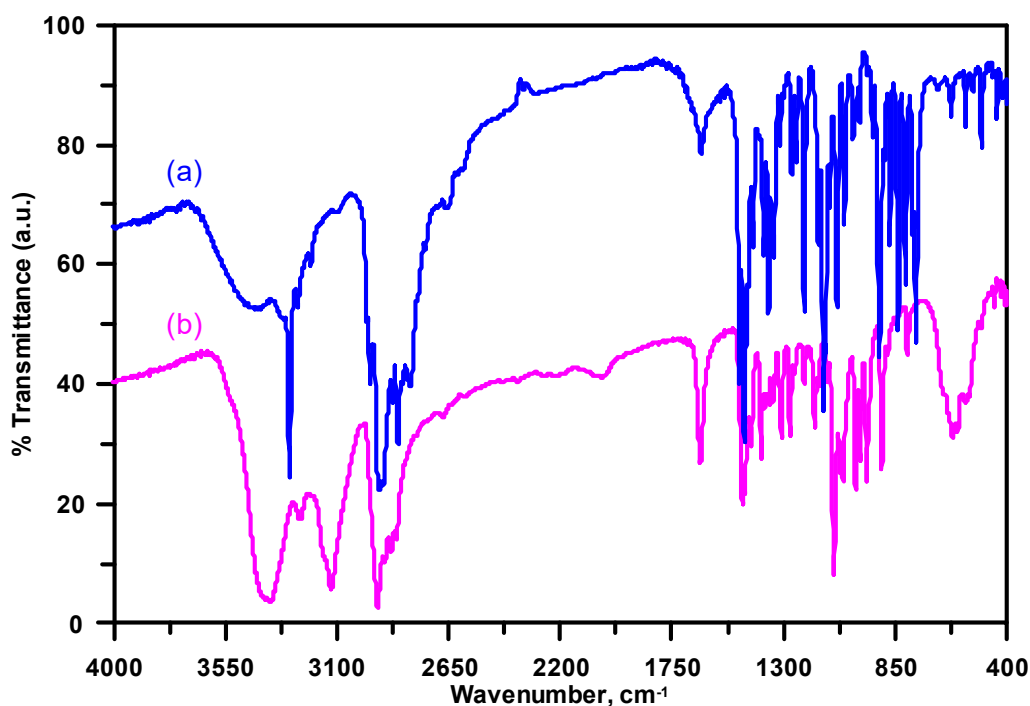

Figure 4. FT-IR spectra of (**a**) free ligand L^1 (blue line) and (**b**) complex (I) (pink line), respectively.

The bands observed in the region 1500–1000 cm^{-1} are assigned to v(C—C) and v(C—N) stretching modes. Two absorptions at 1465 and 1429 cm^{-1} for ligand L^1, and 1476 and 1421 cm^{-1} for complex (I) are attributed to the δ(CH$_2$) stretching modes. IR spectroscopy is useful to assign the *cis* or *trans* geometry of transition metal complexes with cyclam derivatives [5,6]. Generally, the *trans* isomer reveals two groups of bands, overlapping peaks near 890 cm^{-1} due to γ(N—H) wagging mode and one band near 800 cm^{-1} arising from the ϱ(CH$_2$) rocking vibration. However, the cis isomer reveals at least three bands at 890–830 cm^{-1} arising from the γ(N—H) wagging vibration, while the ϱ(CH$_2$) rocking vibration splits into two peaks at 830–790 cm^{-1} [40–43]. In complex (I), two bands at 879

and 845 cm^{-1} and a single absorption band at 801 cm^{-1} are assigned to the γ(N—H) wagging and ϱ(CH$_2$) rocking frequencies, respectively. The three absorptions peaks in the vibrational regions are consistent with the trans-configuration of the constrained cyclam ligand in complex (I). The wagging and rocking deformation bands are not significantly affected by the counter anion or transition metal ion [5,6,40–43].

3.4. Electron Paramagnetic Resonace (EPR) Spectroscopy

The experimental and calculated Cu(II) EPR spectra of the powdered complex (I) recorded at RT are exhibited in Figure 5a,b, respectively. The Cu(II) EPR spectrum with axially symmetric spectral lines and unresolved hyperfine splitting was obtained. The spin Hamiltonian parameters refined by computer simulation of the experimental Cu(II) EPR spectrum is as follows: $g_{\parallel}$ = 2.153 ± 0.002, $g_{\perp}$ = 2.048 ± 0.002. The *g*-factors showed a typical trend of $g_{\parallel} > g_{\perp} > 2.0023$, consisting of the $d_{x^2-y^2}$ ground electronic state, indicating coordination spheres of distorted tetragonal symmetry for central Cu (II) ion. The geometric parameter $G = (g_{\parallel} - 2)/(g_{\perp} - 2) = 3.188$ was calculated, with $G < 4$ indicating the presence some exchange interactions between the Cu(II) ions [37,44]. The EPR spectrum of the Cu(II) complex, which was recorded at a wide magnetic field of 800 mT, confirmed that the typical EPR resonances of Cu(II) dimeric structure are not present. The found spin Hamiltonian parameters are in good accordance with previously presented g-values of similar monomeric Cu(II) complexes [37,44,45].
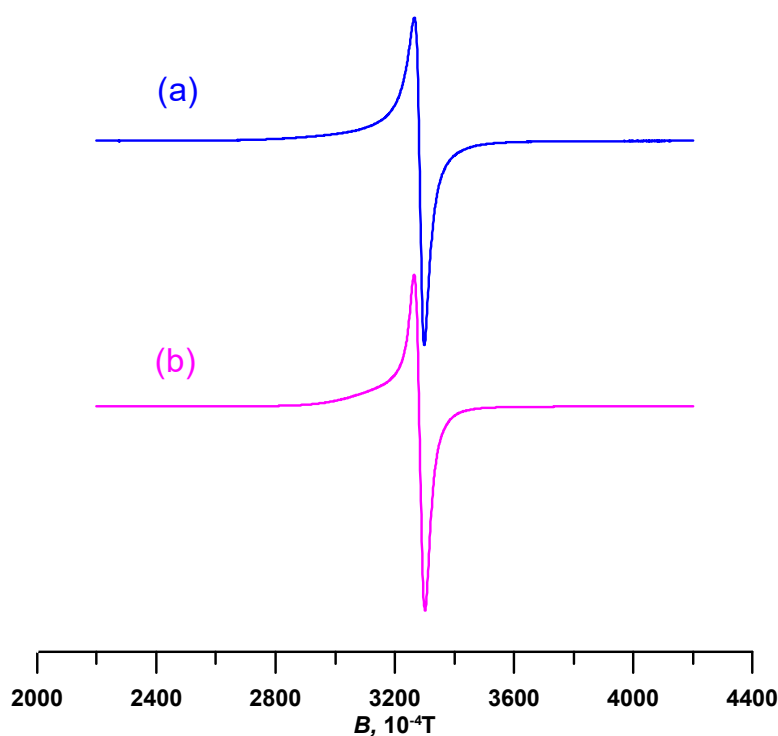

Figure 5. (**a**) Experimental EPR spectrum (blue line) recorded at RT and (**b**) calculated EPR spectrum (pink line) of powdered complex (I).

3.5. Hirshfeld Surface Analysis

Various interactions in the crystal were analyzed by Hirshfeld surfaces (HS) analysis [46] and corresponding the two-dimensional (2D) fingerprint plots [47]. The HS is mapped with d_{norm} and the 2D fingerprint plot of the complex (I) crystal is shown in Figures 6–9.
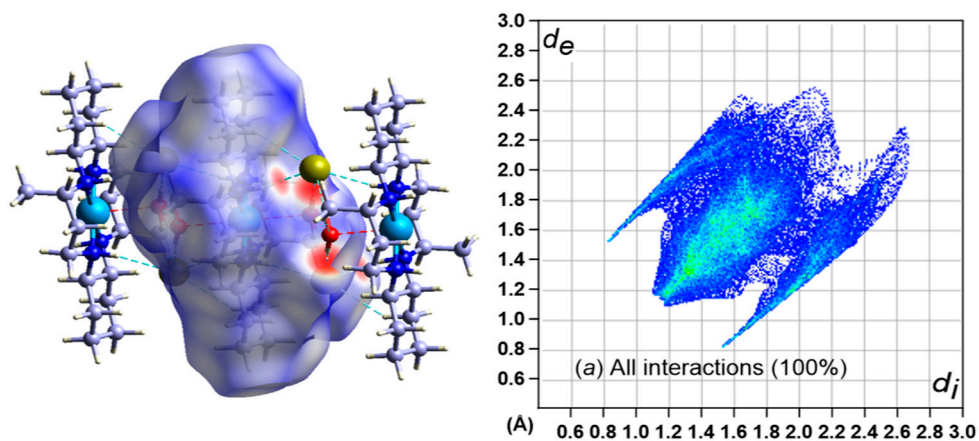
Figure 6. Hirshfeld surface mapped with (**left**) d_{norm}, and 2D fingerprint map (**right**) for all interactions.
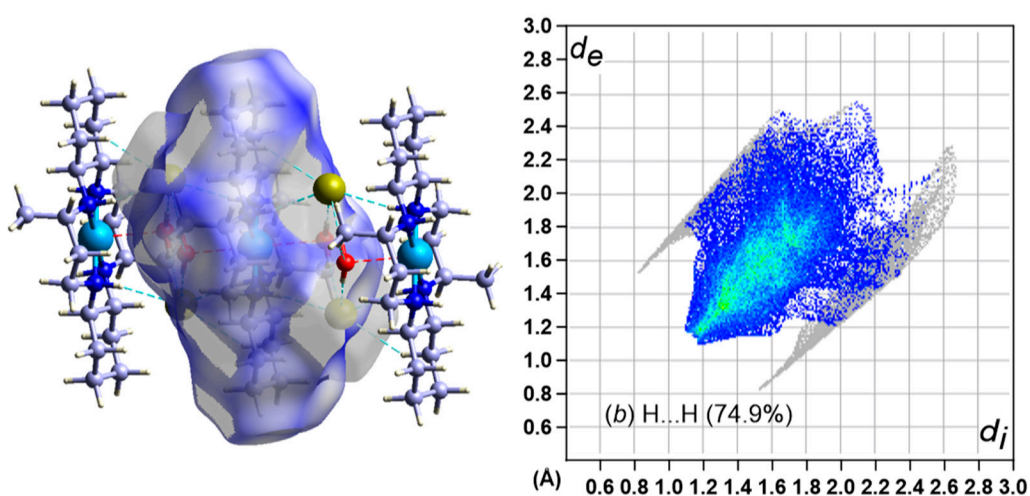

Figure 7. Hirshfeld surface mapped with (**left**) d_{norm}, and 2D fingerprint plot (**right**) for H···H interaction.
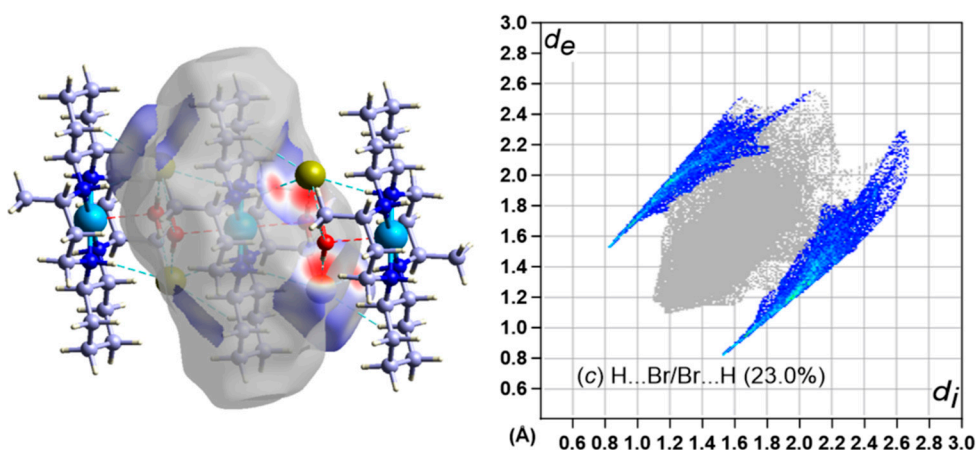

Figure 8. Hirshfeld surface mapped with (**left**) d_{norm}, and 2D fingerprint plot (**right**) for H···Br/Br···H interactions.
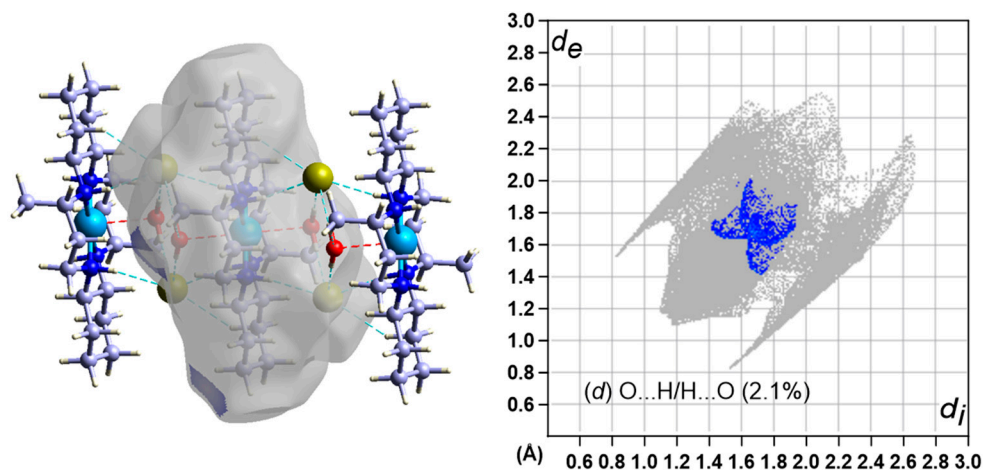
Figure 9. Hirshfeld surface mapped with (**left**) d_{norm}, and 2D fingerprint plot (**right**) for H⋯O/O⋯H interactions.

In the HS with d_{norm} (Figure 7, left), negative values of d_{norm} are denoted by the red color denoting contacts shorter than the sum of the van der Waals (*vdW*) radii of the bonding atoms. The white surface indicates the intermolecular distances that are similar to the *vdW* contacts with d_{norm} equal to zero [48]. In turn, contacts longer than the sum of the associated *vdW* radii with positive d_{norm} values are denoted by the blue color.

Most intermolecular interactions (Figures 7–9, right) are H⋯H (74.9%) and H⋯Br/Br⋯H (23.0%), with some contribution from H⋯O/O⋯H (2.1%). A large number of H⋯H and H⋯/Br⋯H interactions suggest that *vdW* interactions and hydrogen bonding play major roles in the crystal packing [49,50].

4. Conclusions

Electronic absorption and IR spectral properties of complex (I) are in agreement with the crystallographic results, showing that the complex adopted an elongated tetragonal octahedral geometry with a square planar CuN_4 arrangement with two waters occupying axial positions. The uncoordinated bromide anions remain outside the coordination sphere are connected to the water molecules and complex cations through hydrogen bonds. The crystals are stabilized by the hydrogen bonds between hydrogen atoms of secondary N atoms, O atoms of the water molecules, and the Br^- anions. The EPR spectrum is acquired at RT and the *g*-factors, which are refined by computer simulation, exhibit a typical trend: $g_\parallel > g_\perp > 2.0023$. Furthermore, this is in good accord with the $d_{x^2-y^2}$ ground state, indicating a coordination sphere of distorted tetragonal geometry for the Cu(II) ion.

Author Contributions: S.J. prepared the complex and measured IR, UV–Visible spectra. J.M. collected the single-crystal X-ray diffraction data and solved the structure; M.M. measured, analyzed and interpreted the EPR spectrum; M.V. conceived the work, contributed analysis equipment and acted as scientific coordinator; J.-H.C. interpreted the IR and UV-Visible spectra, performed the HS analysis and wrote the manuscript.

Conflicts of Interest: The authors declare no conflict of interest.

References

1. Valks, G.C.; McRobbie, G.; Lewis, E.A.; Hubin, T.J.; Hunter, T.M.; Sadler, P.J.; Pannecouque, C.; De Clercq, E.; Archibald, S.J. Configurationally restricted bismacrocyclic CXCR4 receptor antagonists. *J. Med. Chem.* **2006**, *49*, 6162–6165. [CrossRef] [PubMed]

2. Ronconi, L.; Sadler, P. Using coordination chemistry to design new medicines. *Coord. Chem. Rev.* **2007**, *251*, 1633–1648. [CrossRef]

3. De Clercq, E. Highlights in the discovery of antiviral drugs: A personal retrospective. *J. Med. Chem.* **2010**, *53*, 1438–1450. [CrossRef] [PubMed]

4. Ross, A.; Choi, J.-H.; Hunter, T.M.; Pannecouque, C.; Moggach, S.A.; Parsons, S.; De Clercq, E.; Sadler, P. Zinc(II) Complexes of Constrained Antiviral Macrocycles. *Dalton Trans.* **2012**, *41*, 6408–6418. [CrossRef] [PubMed]

5. Choi, J.-H. Crystal structure and spectroscopic properties of *trans*-bis(nicotinato)(1,4,8,11-tetraazacyclotetradecane)chromium(III) perchlorate. *Inorg. Chim. Acta* **2009**, *362*, 4231–4236. [CrossRef]

6. Subhan, M.A.; Choi, J.-H.; Ng, S.W. Synthesis, crystal structure and spectroscopic properties of (acetylacetonato)(1,4,8,11-tetraazacyclotetradecane)chromium(III) diperchlorate. *Z. Anorg. Allg. Chem.* **2011**, *637*, 2193–2197. [CrossRef]

7. Choi, J.-H.; Tanmaya, T.; Spiccia, L. Syntheses, structural and spectroscopic properties of the copper(II) complexes of constrained macrocyclic ligands. *Z. Anorg. Allg. Chem.* **2012**, *638*, 146–151. [CrossRef]

8. Choi, K.-Y.; Kim, J.C.; Jensen, W.P.; Suh, I.H.; Choi, S.S. Copper(II) and nickel(II) complexes with 3,14-dimethyl-2,6,13,17-tetraazatricyclo[16.4.0.0^{7,12}]docosane, [M(C$_{20}$H$_{40}$N$_4$)]Cl$_2$·2H$_2$O (M = Cu^{II} and Ni^{II}). *Acta Crystallogr.* **1996**, *C52*, 2166–2168.

9. Choi, J.-H.; Ryoo, K.S.; Park, K.M. [3,14-Dimethyl-2,6,13,17-tetraazatricyclo(16.4.0.0^{7,12})docosane-κ^{4}N]bis(perchlorato-κO)copper(II). *Acta Crystallogr.* **2007**, *E63*, m2674–m2675.

10. Choi, J.-H.; Subhan, M.A.; Ng, S.W. [3,14-Dimethyl-2,6,13,17-tetraazatricyclo(16.4.0.0^{7,12})docosane-κ^{4}N]bis(nitrato-κO)copper(II). *Acta Crystallogr.* **2012**, *E68*, m190.

11. Choi, J.-H.; Suzuki, T.; Kaizaki, S. [3,14-Dimethyl-2,6,13,17-tetraazatricyclo(16.4.0.0^{7,12})docosane-κ^{4}N]dinitratocopper(II) trihydrate. *Acta Crystallogr.* **2006**, *E62*, m2383–m2385.

12. Subhan, M.A.; Ryoo, K.S.; Choi, J.-H. Crystal structure and spectroscopic properties of [3,14-dimethyl-2,6,13,17-tetraazatricyclo(16.4.0.0^{7,12})docosane]copper(II) dithiocyanate dihydrate. *Int. J. Chem. Sci.* **2015**, *13*, 593–604.

13. Subhan, M.A.; Ng, S.W.; Lee, C.S.; Choi, J.-H. Synthesis, crystal structure, and spectroscopic properties of isothiocyanato[3,14-dimethyl-2,6,13,17-tetraazatricyclo(16.4.0.0^{7,12})docosane]copper(II) thiocyanate. *J. Struct. Chem.* **2017**, *58*, 742–749. [CrossRef]

14. Choi, K.-Y. Synthesis and crystal structure of a macrocyclic azidotetraamine copper(II) complex. *J. Chem. Crystallogr.* **1998**, *28*, 875–878. [CrossRef]

15. Choi, J.-H.; Clegg, W.; Harrington, R.W. Crystal structure of [2,13-dibenzyl-5,16-dimethyl-2,6,13,17-tetraazatricyclo(14,4,0,0^{7,12})docosane]copper(II) diperchlorate. *J. Chem. Crystallogr.* **2010**, *40*, 80–84. [CrossRef]

16. Choi, J.-H.; Clegg, W.; Gary, G.S. Synthesis, crystal structure and spectroscopic properties of [2,13-bis(1-naphthalenylmethyl)-5,16-dimethyl-2,6,13,17-tetraazatricyclo(14,4,0,0^{7,12})docosane]copper(II) diperchlorate acetonitrile disolvate. *Z. Anorg. Allg. Chem.* **2010**, *636*, 1612–1616. [CrossRef]

17. Lim, J.H.; Kang, J.S.; Kim, H.C.; Koh, E.K.; Hong, C.S. Synthesis, crystal structures, and magnetic properties of cyano-bridged honeycomb like layers M^V-Cu^{II} (M=Mo, W) chelated by a macrocyclic ligand. *Inorg. Chem.* **2006**, *45*, 7821–7827. [CrossRef] [PubMed]

18. Moncol, J.; Mazúr, M.; Valko, M.; Choi, J.-H. Synthesis, structural characterization, EPR spectroscopy and Hirshfeld surface analysis of novel Cu^{2+} doped 3,14-diethyl-2,13-diaza-6,17-diazoniatricyclo(16.4.0.0^{7,12})docosane diperchlorate. *Acta Crystallogr.* **2019**, *C75*, 612–622. [CrossRef] [PubMed]

19. Choi, J.-H.; Subhan, M.A.; Ng, S.W. Syntheses, crystal structures and spectroscopic properties of [Cu(L)(NO$_3$)$_2$] and [Cu(L)(H$_2$O)$_2$](SCN)$_2$ with 3,14-diethyl-2,6,13,17-tetraazatricyclo(16.4.0.0^{7,12})docosane (L). *J. Coord. Chem.* **2012**, *65*, 3481–3491. [CrossRef]

20. Subhan, M.A.; Choi, J.-H. X-ray structure and spectroscopy of novel *trans*-[Ni(L)(NO$_3$)$_2$] and [Ni(L)](ClO$_4$)$_2$·2H$_2$O complexes. *Spectrochim. Acta Part A* **2014**, *123*, 410–415. [CrossRef] [PubMed]

21. Lim, I.-T.; Kim, C.-H.; Choi, K.-Y. Synthesis and structural characterization of nickel(II) complexes of 3,14-diethyl-2,6,13,17-tetraazatricyclo(14.4.0.0^{7,12})docosane with inorganic salts. *Polyhedron* **2015**, *100*, 43–48.

22. Subhan, M.A.; Moon, D.; Choi, J.-H. Synthesis, crystal structure determination, and spectroscopic characterization of [2,13-dibenzyl-5,16-diethyl-2,6,13,17-tetraazatricyclo(16.4.0.0^{7,12})docosane]copper(II) dinitrate. *Main Group Chem.* **2017**, *16*, 27–36. [CrossRef]

23. Jimenez, D.; Martinez-Manez, R.; Sancenon, F.; Ros-Lis, J.V.; Soto, J. A new chromo-chemodosimeter selective for sulfide anion. *J. Am. Chem. Soc.* **2003**, *125*, 9000–9001. [CrossRef] [PubMed]

24. Martinez-Manez, R.; Sancenon, F. Fluorogenic and chromogenic chemosensors and reagents for anions. *Chem. Rev.* **2003**, *103*, 4419–4476.

25. Kang, S.G.; Kweon, J.K.; Jung, S.K. Synthesis of new tetraaza macrocyclic ligands with cyclohexane ring and their Ni(II) and Cu(II) complexes. *Bull. Korean Chem. Soc.* **1991**, *12*, 483–487.

26. Moon, D.; Choi, J.-H. Crystal structure of 3,14-dimethyl-2,6,13,17-tetraazoniatricyclo(16.4.0.0^{7,12})docosane tetrachloride tetrahydrate from synchrotron X-ray data. *Acta Crystallogr.* **2018**, *E74*, 1039–1041.

27. Mazur, M.; Valko, M.; Klement, R.; Morris, H. Quantitative EPR spectroscopy with a TE$_{104}$ double rectangular cavity. Part 1. A simple alignment procedure for the precision positioning of the sample. *Anal. Chim. Acta* **1996**, *333*, 249–252. [CrossRef]

28. Thiele, H.; Etstling, J.; Such, P.; Hoefer, P. *WINEPR*; Bruker Analytic Gmb: Rheinstetten, Germany, 1992.

29. Weber, R.T. *WINEPR SimFonia*; EPR Division, Bruker Instr. Inc.: Billerica, MA, USA, 1995.

30. Sheldrick, G.M. SHELXT-Integrated space-group and crystal-structure determination. *Acta Crystallogr.* **2015**, *A71*, 3–8. [CrossRef] [PubMed]

31. Sheldrick, G.M. Crystal structure refinement with SHELXL. *Acta Crystallogr.* **2015**, *C71*, 3–8.

32. Koziskova, J.; Hahn, F.; Richter, J.; Kozisek, J. Comparison of different absorption corrections on the model structure of tetrakis(μ2-acetato)diaquadicopper(II). *Acta Chim. Slovaca* **2016**, *9*, 136–140. [CrossRef]

33. Putz, H.; Brandenburg, K. *DIAMOND-3*; University of Bonn: Bonn, Germany, 2014.

34. Turner, M.J.; McKinnon, J.J.; Wolff, S.K.; Grimwood, D.J.; Spackman, P.R.; Jayatilaka, D.; Spackman, M.A. CrystalExplorer17.5. The University of Western Australia. 2017. Available online: http://crystalexplorer.scb.uwa.edu.au/ (accessed on 27 June 2019).

35. McKinnon, J.J.; Spackman, M.A.; Mitchell, A.S. Novel tools for visualizing and exploring intermolecular interactions in molecular crystals. *Acta Crystallogr.* **2004**, *B60*, 627–668. [CrossRef]

36. McKinnon, J.J.; Jayatilaka, D.; Spackman, M.A. Towards quantitative analysis of intermolecular interactions with Hirshfeld surfaces. *Chem. Commun.* **2007**, 3814–3816. [CrossRef]

37. Hathaway, B.J.; Billing, D.E. The electronic properties and stereochemistry of mononuclear complexes of copper(II) ion. *Coord. Chem. Rev.* **1970**, *5*, 43–207. [CrossRef]

38. Hathaway, B.J.; Hodgson, P.G. Copper-ligand bond-lengths in axial complexes of the copper(II) ion. *J. Inorg. Nucl. Chem.* **1973**, *35*, 4071–4081. [CrossRef]

39. Lever, A.B.P. *Inorganic Electronic Spectroscopy*, 2nd ed.; Elsevier: Amsterdam, The Netherlands, 1984.

40. Nakamoto, K. *Infrared and Raman Spectra of Inorganic and Coordination Compounds, Part A: Theory and Applications in Inorganic Chemistry; Part B: Applications in Coordination, Organometallic, and Bioinorganic Chemistry*, 6th ed.; John Wiley & Sons: New York, NY, USA, 2009.

41. Choi, J.-H.; Oh, I.-G.; Suzuki, T.; Kaizaki, S. Crystal structure and spectroscopic properties of oxalato(1,4,8,11-tetraazacyclotetradecane)chromium(III) perchlorate. *J. Mol. Struct.* **2004**, *694*, 39–44. [CrossRef]

42. Choi, J.-H. Spectral properties and ligand field analysis of *cis*-dinitrito(1,4,8,11-tetraazacyclotetradecane)chromium(III) nitrate. *Chem. Phys.* **2000**, *256*, 29–35. [CrossRef]

43. Choi, J.-H. Spectroscopic properties and ligand field analysis of *cis*-diazido(1,4,8,11-tetraazacyclotetradecane)chromium(III) azide. *Spectrochim. Acta Part A* **2000**, *56*, 1653–1660. [CrossRef]

44. Choi, J.-H.; Oh, I.-G.; Linder, R.; Schönherr, T. Electronic spectroscopy and ligand field analysis of *cis*-carbonato(*rac*-5,5,7,12,12,14-hexamethyl-1,4,8,11-tetraazacyclotetradecane)chromium(III) chloride. *Chem. Phys.* **2004**, *297*, 7–12. [CrossRef]

45. Hathaway, B.J.; Tomlinson, A.A.G. Copper ammonia complexes. *Coord. Chem. Rev.* **1970**, *5*, 1–43. [CrossRef]

46. Goodman, B.A.; Raynor, J.B. Electron spin resonance of transition metal complexes. *Adv. Inorg. Chem. Radiochem.* **1970**, *13*, 135–362.
47. Spackman, M.A.; Jayatilaka, D. Hirshfeld surface analysis. *CrystEngComm* **2009**, *11*, 19–32. [CrossRef]
48. Moon, D.; Tanaka, S.; Akitsu, T.; Choi, J.-H. Molecular structure, spectroscopic properties, and Hirshfeld surface analysis of chlorobis(*N*-methyl-1,3-propanediamine)copper(II) tetrafluoroborate and azidobis(2,2-dimethyl-1,3-propanediamine)copper(II) azide. *J. Mol. Struct.* **2018**, *1154*, 338–347; Erratum in **2018**, *1168*, 329.
49. Hathwar, V.R.; Sist, M.; Jørgensen, M.R.V.; Mamakhel, A.H.; Wang, X.; Hoffmann, C.M.; Sugimoto, K.; Overgaard, J.; Iversen, B.B. Quantitative analysis of intermolecular interactions in orthorhombic rubrene. *IUCrJ* **2015**, *2*, 563–574. [CrossRef] [PubMed]
50. Spackman, M.A.; McKinnon, J.J.; Jayatilaka, D. Electrostatic potentials mapped on Hirshfeld surfaces provide direct insight into intermolecular interactions in crystals. *CrystEngComm* **2008**, *10*, 377–388. [CrossRef]